

STUDY ON PID PERFORMANCE DEGRADATION BASED ON PASSIVATION MATERIALS SUCH AS ALUMINA/SILICON NITRIDE SiN CRYSTALLINE SILICON SOLAR CELLS

by

**Huayun GE^{a,b}, Xing LI^{a,b}, Chunlin GUO^{a,b},
Ke TAO^c, and Rui JIA^{a,b*}**

^aInstitute of Microelectronics of Chinese Academy of Sciences, Beijing, China

^bSchool of Integrated Circuits, University of Chinese Academy of Sciences, Beijing, China

^cSchool of Integrated Circuit Science and Engineering, Tianjin University of Technology,
Tianjin, China

Original scientific paper

<https://doi.org/10.2298/TSCI221022222G>

Solar energy is a pure and reproducible energy. China has paid more and more consideration to the investigation and employment of solar energy. The investigation focuses on the phenomenon of PID capability degradation of inactivation mediums for instance alumina/silicon nitride in transparent silicon high-efficiency solar cells. Through the laboratorial investigation on the effect of individual inactivation membrane processes on the PID damping behavior, it is found that the deposition approach of silicon oxide and silicon nitride inactivation membranes on the surface of transparent silicon cells directly affects the PID damping. Excellent anti-PID capability; single-layer silicon oxide membrane with the same thickness has better anti-PID capability than silicon nitride membrane. Double-layer silicon oxide/silicon nitride superimposed membrane with the enhancement of refractive index, the anti-PID damping capability gradually enhancements, and better anti-PID capability than monolayer silicon nitride. Investigation on the PID capability damping of inactivation mediums is of great significance to further the capability of solar cells and help to further the effective employment of solar energy.

Key words: solar cell, silicon nitride, silicon oxide, inactivation material, PID damping

Introduction

In the 21st century, three major issues, for instance energy poverty, environmental pollution, and GHG, have prompted the rapid development of reproducible pure energy [1]. Among them, solar energy has the *infiniteness* of reserves, the universality of existence, the pureness of employment, and the economy of employment [2]. Solar generate electricity is uncoupled into photothermal generate electricity and electro-optic generate electricity. Electro-optic generate electricity is a science that rapidly converts light energy into electrical energy by using the electro-optic effect of the semiconductor interface. The main component of elec-

*Corresponding author, e-mail: rui_jia100@126.com

tro-optic generate electricity is solar cells, which can be uncoupled into amorphous silicon, transparent silicon and compound solar cells according to individual mediums. Among them, transparent silicon solar cells and components are currently the mainstream of solar cells, and its market share has remained above 90% in recent years [3]. The International Energy Agency predicts that the world's electro-optic generate electricity will take up 2% of the amount generate electricity in 2020, and will take up 20% to 28% of the amount generate electricity in 2040 [4]. The EU Joint investigation Center predicts that by 2030, the proportion of reproducible energy in the amount energy configuration will take up leavings behind 30%, and solar electro-optic generate electricity will reach leave behind 10% in the world's amount power provision [5]. In 2040, reproducible energy will take up leavings behind 50% of the amount energy configuration, and solar electro-optic generate electricity will take up leavings behind 20% of the world's amount power provision. By the end of the 21st century, reproducible energy will take up leavings behind 80% of the amount energy configuration. Electro-optic generate electricity will take up leavings behind 60% of the world's amount power provision [6, 7]. It can be seen that the global electro-optic market demand is huge, and electro-optic generate electricity is an industry with good development prospects.

Related work

The investigation on the PID capability damping of solar cells and inactivation mediums has been extremely valued by many related professionals, and investigations at home and abroad have also conducted in-depth investigation on this science. Liang *et al.* [8] evaluated the inactivation effect of some inactivation mediums on lead-contaminated soil using soil pH value, effective lead content, lead form and bioactivity coefficient as indicators. The laboratorial consequences showed that blast furnace scoria and fly ash could enhancement soil pH, corncob biochar and phosphate manure could reduce soil pH, and the soil valid lead content of blast furnace scoria and phosphate manure treatment group was significantly lower than that of other treatments. In addition, blast furnace scoria and phosphate manure can significantly convert non-surplus lead to residual lead. Using a 1-D solar cell capacitance simulator simulation program, Mishra *et al.* [9] simulated PID triggering of thin-membrane solar cells with individual absorber layers. The effect of PID on electrical parameters and overall capability characteristics is explained by appropriately matrixing defect states in semiconductor layers and at interfaces. For the detailed analysis of thin-membrane solar cells, the hierarchical distribution is also varied, and a thorough analysis of parameter drop is also done. In addition, the investigation on quantum efficiency and energy band diagram is also carried out, and the graph calculation is realized in MATLAB software. Kivik *et al.* [10] measured the real and imaginary parts of the battery impedance by the PEIS approach. The consequences of impedance changes during discharge and charge are plotted as a Nyquist diagram. During the charging and discharging process of solar cells, important values for instance ohmic resistance (RS), charge transfer resistance (CT), electric double layer capacitance (CDL), and Warburg coefficient, σ , were found. Shubhra *et al.* [11] proposed a control approach based on a normalized gradient adaptive regularization factor neural filter for a three-phase grid-connected solar electro-optic cell energy storage microgrid system. This nervous filter-based current controller furthers the dynamic response of the proposed scheme and feeds active power to the utility grid by exploiting the feed forward term of solar electro-optic power in variable atmospheric scenarios. The microgrid system is simulated by MATLAB/Simulink software, and the capability of the system is verified to be satisfactory under various operating conditions.

Salim *et al.* [12] established a stochastic optimization matrix to budget a budget solar cell storage system. For larger matrix's, the study utilizes a LaGrange relaxation scheme to further it. To further velocity up the LaGrange approach, an asymptotic hedging algorithm is embedded in the sub gradient iterations of the LaGrange relaxation. Several enhancements to the progressive hedging algorithm are studied and the consequences of the bundling scenario are found to be within the best bounds. Zare *et al.* [13] combined solar dryers with olive croppers to use solar energy to reduce energy loss. After the olives are separated from the tree by using a designed and built cropper, a solar dryer is used to hold the olives for a final inspection of the olives for any damage. The consequences of the study show that the olive cropper can separate up to 92% of the olive fruit. The olive cropper was also found to have a crop efficiency of 29.47. Furthermore, evaluations of solar dryers have highlighted that enhancements in inlet air temperature and velocity lead to rapid reductions in olive moisture. Cagle *et al.* [14] used floating electro-optic solar devices to save land, further water surface employment and realize water surface conversion. Noorollahi *et al.* [15] propose a space-based integrated matrix of regional solar science potential. First, collect data related to the sun and select appropriate criteria and assessment techniques based on existing data. Then, evaluate the academic feasible of solar energy and map the solar irradiation. In addition, the technical feasible of various solar technologies was assessed in this investigation area. These technologies comprise concentrated solar power and electro-optics in power plant applications, and rooftop electro-optic panels and solar water heaters in general applications. The consequences showed that the Kurdistan province has a feasible capacity of 691 MW of solar PV plants and 645 MW of CSP plants. In the case of using solar water heaters, the fuel consumption of 283 million cubic meters of natural gas and 1.2 million liters of gasoline can be saved. The application of domestic electro-optic generate electricity will save 10.2 MW of electricity.

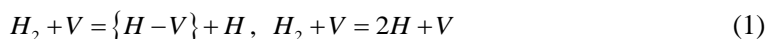
From the investigation on solar energy and inactivation mediums by scholars at home and abroad, it can be seen that good application consequences have been achieved in many fields. For purpose of furthering and stabilizing the PID capability of inactivation mediums in transparent silicon high-efficiency solar cells, a more in-depth analysis was carried out.

Investigation on PID damping based on inactivation mediums for transparent silicon high-efficiency solar cells

Influence of inactivation membrane science on PID damping of transparent silicon battery

The amorphous membrane of transparent silicon battery has the effect of weakening reflection and inactivation, so it can also be called inactivation membrane, and its configuration is related to short-distance chylic bonds [16, 17]. There are basically two kinds of inactivation membranes that are more common in daily life, namely silicon nitride membrane and silicon oxide membrane [18, 19]. They are characterized by good chylic stability, inactivation, optical and mechanical properties [20]. The refractive index of the silicon nitride membrane is $n = 1.8\sim 2.4$, and the Si/N ratio will affect its fluctuation in this range. Among them, the refractive index is conversely proportional to the nitrogen atom content and proportional to the silicon atom. In addition to nitrogen and silicon atoms, the deposition temperature also affects the refractive index, which is proportional to the relationship between them. The reason for this effect is that the enhancement in temperature enhances the density of the membrane. The forbidden band width, E_g , of amorphous silicon nitride is about 5 eV. The forbidden band of this level is already relatively wide, and there will be no thermal excitation of the valence band

and the guide band. There is a trap energy level about 1.5 eV below the bottom of the conduction band. Under the action of high temperature and strong electric field, electrons on the trap energy level are excited into the conduction band, causing a tiny current through the silicon nitride membrane. The cyclic stability of the silicon nitride membrane is very good. For transparent Si₃N₄, other acids and bases are almost inactive except for hydrofluoric acid. Silicon nitride membrane can actually prevent the diffusion of impurities for instance B, P, Na, As, Sb, Ge, Al, Zn, *etc.*, peculiarly for Na⁺. In addition to the Si-N component, the silicon nitride membrane also contains considerable weakly bonded hydrogen and trace oxygen. The H content of the membrane is relatively high, up to 20-30% (atomic percent). Too high H content has adverse effects on the configuration, density, refractive index, stress and corrosion rate of the membrane. But an appropriate amount of H will passivate the surface. The interface state density of charges at the interface of silicon and silicon nitride is high, and this interface state acts as a trap or recombination center for carriers near the interface. Hydrogen inactivation can actually reduce the surface recombination velocity and enhancement the minority carrier lifetime, thereby improving the solar cell efficiency. Hydrogen inactivation is done at the same time as the deposition of the Si₃N₄ membrane. When Si₃N₄ is stored by PECVD, a part of the hydrogen will remain in the Si₃N₄ membrane due to the presence of hydrogen in the gas produced by the reaction. In the process of high temperature, this part of hydrogen will be released from Si₃N₄, diffused into silicon, and finally combined with dangling bonds to play an inactivation role. The advantage of PECVD hydrogen inactivation is that it can be completed at the same time as the deposition of the SiN_x anti-reflection layer, reducing process steps. The disadvantage is that the plasma will cause certain damage to the silicon surface. Investigation in recent years has shown that defects (vacancies) in silicon play a decisive role in the decomposition of hydrogen molecules, which can be expressed:



where V represents a vacancy. The vacancies can dissociate hydrogen molecules and can enhance the diffusion of hydrogen. In this way, hydrogen atoms and hydrogen-vacancy pairs can diffuse rapidly in the silicon, thereby acting as inactivation. When light hits the surface of a silicon wafer, about one-third of the light is lost due to reflection. If there are one or more suitable thin membranes on the silicon surface, the light reflection can be greatly reduced by using the principle of thin membrane interference cancellation, the short-circuit current and output of the battery will be greatly enhanced, and the efficiency will also be greatly improved. The principle of the anti-reflection coating is that the light irradiated on the silicon wafer cannot be completely absorbed by the silicon due to reflection. The size of the reflection percentage depends on the refractive index of silicon and the external transparent medium. At normal incidence, the reflectivity of the silicon wafer surface is shown:

$$R = \left(\frac{n_{\text{si}} - n_o}{n_{\text{si}} + n_o} \right)^2 \quad (2)$$

where the refractive index of silicon is expressed as n_{si} , and its value is 1 in vacuum or atmosphere, the refractive index of the external medium is expressed as n_o . If a transparent dielectric membrane is prepared on the outside of silicon, since the reflected light on the two interfaces of the dielectric membrane interferes with each other, the reflectivity can be reduced in a wide wavelength range.

The reflectance at this time is shown:

$$R = \frac{r_1^2 + r_2^2 + 2r_1r_2 \cos \Delta}{1 + r_1^2 + r_2^2 + 2r_1r_2 \cos \Delta} \quad (3)$$

where the Fresnel reflection coefficients at the external medium-membrane and membrane-silicon interfaces are r_1 and r_2 and it can be expressed:

$$r_1 = \frac{n_o - n}{n_o + n}, \quad r_2 = \frac{n - n_{si}}{n + n_{si}} \quad (4)$$

where the external medium is expressed as n_o , the membrane layer is expressed as n , and the refractive index of silicon is expressed as n_{si} . The phase angle caused by the membrane thickness is Δ , which can be expressed:

$$\Delta = \frac{4\pi}{\lambda_0} nd \quad (5)$$

where the wavelength of incident light is expressed as λ_0 , the actual thickness of the membrane is expressed as d , and the optical thickness of the membrane is expressed as nd . If the optical thickness of the membrane layer at this time is $\lambda_0/4$ when the light $nd = \lambda_0/4$ with the wavelength is perpendicularly incident, it can be expressed as λ_0 , then the eq. (6) can be obtained:

$$R\lambda_0 = \left(\frac{n^2 - n_o n_{si}}{n^2 + n_o n_{si}} \right)^2 \quad (6)$$

When $R\lambda_0 = 0$, the reflection loss can be reduced to the minimum, then eq. (7) will appear:

$$n = \sqrt{n_o n_{si}} \quad (7)$$

Therefore, the refractive index of the anti-reflection coating required for a given wavelength, λ_0 , can be obtained by eq. (7), and the optimal optical thickness of the coating layer is one-fourth of the wavelength. At this time, the reflectivity is the smallest, close to zero. But when the wavelength deviates from λ_0 , the reflectivity will be enhanced. For the purpose of enhancing the battery output as much as possible, a reasonable design wavelength λ_0 should be taken first. This requires consideration of two aspects, the composition of the solar spectrum and the relative spectral response of the cell. The peak of the spectral energy of the terrestrial solar energy is at the wavelength of 0.5 μm , while the relative response peak of the silicon solar cell is at the wavelength of 0.8-0.9 μm . Therefore, the wavelength range with the best anti-reflection effect is 0.5-0.7 μm , and $\lambda_0 = 0.6 \mu\text{m}$ is desirable. A silicon solar cell with an anti-reflection coating of this thickness appears dark blue to the naked eye. At this time, the refractive index of silicon is $n_{Si} = 3.9$, so if the battery is directly exposed to vacuum or used in the atmosphere, the refractive index of the most matching anti-reflection coating can be expressed:

$$n = \sqrt{3.9} \approx 1.97 \quad (8)$$

The membrane thickness and refractive index are the two most important parameters of the anti-reflection inactivation coating. How to match the two parameters to get the best capability needs to be debugged in the process.

Sample preparation and testing of individual battery inactivation membrane processes

The investigation uses conventional P-type polysilicon in the production line and the same ingot silicon wafer. Two communities of silicon wafers were selected and coated with individual deposition techniques of silicon oxide inactivation membrane and individual deposition techniques of silicon nitride inactivation membrane, and then the minority carrier life test was carried out, and then they were made into batteries and small components for PID test. The influence of individual deposition techniques of silicon inactivation membrane on PID damping was compared and analyzed. After the silicon wafer was pured and diffused, the silicon nitride membrane was made by using the tubular PECVD equipment of CT company in Germany. The deposition temperature was 375 °C. The membrane thickness was 85 nm by changing the flow ratio of silane and ammonia. Five communities of instances in 2.15 and 2.2, each group of instances has 50 pieces. The silicon oxide membrane was prepared by Qixing Huachuang thermal oxidation furnace equipment. When $n = 1.416$, the deposition time was 50 minutes at 950 °C, 990 °C, 1025 °C, and 1040 °C, separately. The refractive index and membrane thickness were then measured using a spectroscopic ellipsometer. After the individual process instances are made into components, the PID test is carried out. The PID test conditions are temperature 85 °C, humidity 85%, reverse electric tension -1000 V, 96 h. Finally, use an IV tester to test the electrical capability parameters. At the same time, EL was used to analyze the image comparison before and after the PID test, and SEMILAB's WT2000 was used to conduct the VQ test and the self-regulating steady-state residual electric tension test on the sample.

Investigation and analysis of PID capability damping of transparent silicon battery inactivation membrane process

Influence of individual inactivation membrane deposition techniques on PID damping

The techniques of depositing silicon oxide inactivation membranes in the electro-optic industry basically comprise high-electric tension discharge ozone approach and high-temperature dry oxygen oxidation. The investigation divides ozone-oxidized silicon wafers into four communities of instances, and changes the oxidation time by mastering the belt velocity. The oxidation time is 2 seconds, 3 seconds, 4 seconds, and 5 seconds, separately. The life of the silicon wafer is tested by Semilab equipment. The life of the tested silicon wafer is shown in fig. 1. As shown, blue-green represents high minority lifetime, and red-yellow represents low minority lifetime.

Thermal oxidation is uncoupled into four communities of instances, the same oxidation time and individual oxidation temperature. The oxidation time is 15 minutes, and the oxidation temperature is 950 °C, 990 °C, 1025 °C, 1040 °C, using Qixing Huachuang diffusion furnace for oxidation. The thicknesses are 19 nm, 37 nm, 45 nm, and 83 nm, separately. Using Semilab equipment to test the lifetime of silicon wafers, the minority carrier lifetime diagram of the tested silicon wafers is shown in fig. 2.

It can be seen from figs. 1 and 2, the color distribution of the lifetime of a single silicon wafer shows that the deposition of the two types of silicon oxide membranes is relatively uniform, and only the edge part of the second group has a lower lifetime, which is related to the selected area of the silicon wafer. With the enhancement of oxidation time, the membrane thickness of ozone oxidized silicon wafer enhances, and the minority carrier lifetime shows a downward trend. The minority carrier lifetime of the thermally oxidized silicon wafer decreases

with the enhancement of the thickness of the stored silicon oxide membrane. By collating the effects of the two oxidation inactivation membrane techniques on the PID damping, it is found that, as shown in fig. 3.

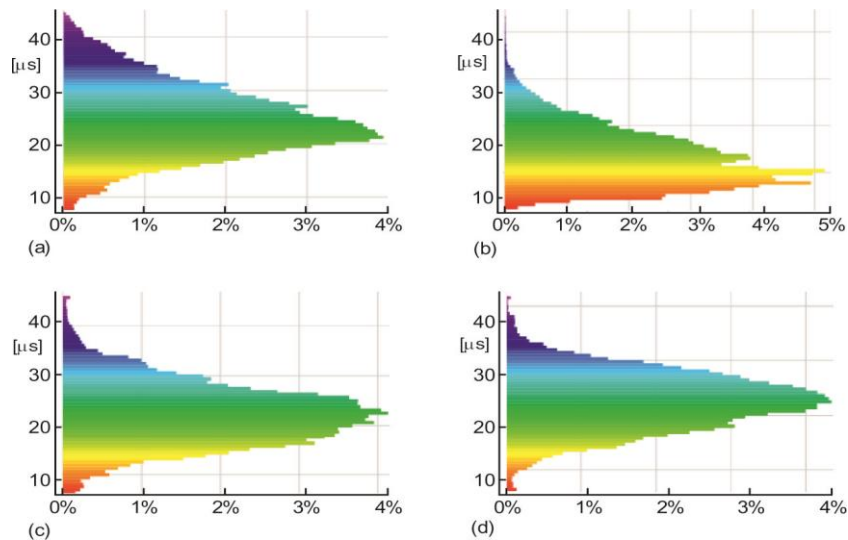


Figure 1. Minority carrier lifetime spectra of silicon wafers with individual deposition times by ozone approach; (a) 2 seconds, (b) 3 seconds, (c) 4 seconds, and (d) 5 seconds

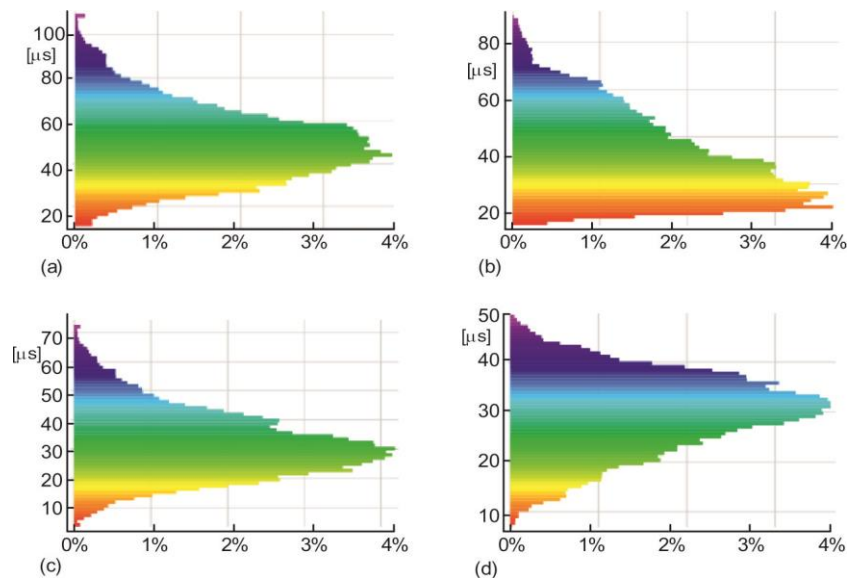


Figure 2. Minority carrier lifetime spectra of silicon wafers with individual deposition times by thermal oxidation approach; (a) 950 °C, (b) 990 °C, (c) 1025 °C, and (d) 1040 °C

It can be seen from fig. 3 that the thermal oxidation inactivation membrane has a better effect than the ozone normal temperature oxidation inactivation membrane, and the PID damping of the small components is relatively low. The most commonly used silicon nitride

coating techniques in the former electro-optic industry are tubular PECVD and plate PECVD. Using tube P and plate P to deposit instances with the same membrane thickness and individual refractive indices, the membrane thickness is 85 nm, and the refractive indices are 2.05, 2.10, and 2.15, separately. By collating the influence of the two-silicon nitride inactivation membrane techniques on the PID damping, it is found that the capability before and after the PID test of the tubular PECVD and plate PECVD deposition silicon nitride membrane fabrication components is shown in tab. 1.

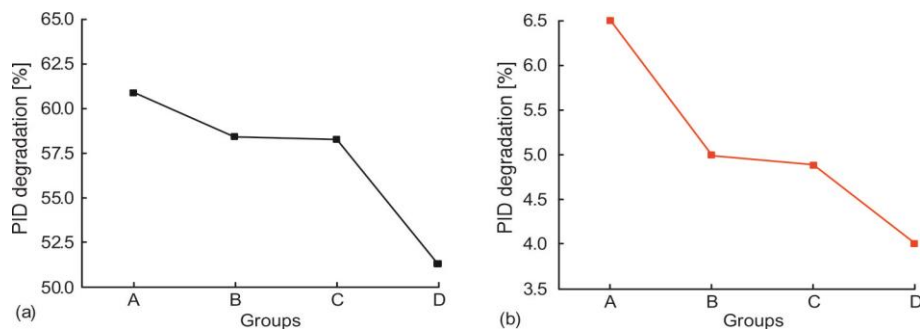


Figure 3. Comparison of PID damping of components with individual oxidation techniques; (a) O₃ oxidization and (b) thermal oxidization

Table 1. Tubular PECVD and plate PECVD deposition of silicon nitride inactivation membrane components before and after PID test capability

	Refractive index	2.05	2.10	2.15
Tubular PECVD	Efficiency before PID [%]	17.91	17.69	17.10
	Efficiency after PID [%]	15.16	15.74	16.38
	Damping [%]	15.35	11.02	4.21
Plate PECVD	Efficiency before PID [%]	17.16	17.12	17.88
	Efficiency after PID [%]	1.41	13.01	16.12
	Damping [%]	91.78	24.01	9.84

Table 1 shows that when the silicon nitride refractive index is 2.05, 2.10, and 2.15, the PID damping of tubular PECVD components is 5.35%, 11.02%, and 4.21%, respectively, and that of plate PECVD components is 91.78%, 24.01%, and 9.84%, respectively. It can be seen that, with the increase of refractive index, the PID damping of silicon nitride inactivated membrane elements stored by the two processes shows a decreasing trend. However, compared with the silicon nitride passive film stored by the plate PECVD, the damping of the silicon nitride passive film stored by the tubular PECVD is lower and has higher anti PID capability.

Influence of single-layer silicon oxide/silicon nitride inactivation membrane on PID damping

Five communities of test instances with refractive indices of 2.0, 2.05, 2.1, 2.15, and 2.2 stored by tubular PECVD were made into cells and packaged into small components for PID testing in a double 85 laboratorial box. The average efficiency before and after the test was compared, for instance shown in tab. 2.

It can be seen from tab. 2 that the efficiency of the module has decreased to varying degrees after the PID test. As the refractive index changed from 2.0 to 2.2, the PID damping decreased from 81.71% to 1.46%. The SiN_x refractive index enhancement and decreased, peculiarly when the refractive index reached from 2.05 to 2.15, the PID decay decreased rap-

idly, and then gradually became stable with the enhancement of the refractive index. Figure 4 shows the test VQ consequences of single-layer silicon nitride membranes with individual refractive indices.

Table 2. Comparison of the average efficiency of five communities of test instances before and after testing

Refractive index	2.00	2.05	2.10	2.15	2.20
Cell efficiency [%]	17.60	17.60	17.60	17.60	17.20
Efficiency before PID [%]	16.68	16.73	16.67	16.61	16.35
Efficiency after PID [%]	3.05	11.53	13.22	16.14	16.11
Damping [%]	81.71	31.08	20.69	2.82	1.46

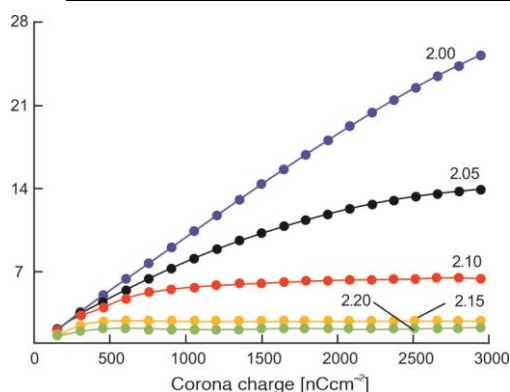


Figure 4. Variation of VQ with refractive index of monolayer silicon oxide membrane

From fig. 4, when the charging capacity is continuously enhanced from 0 nC/cm² to 3000 nC/cm², and the surface electric tension of the silicon nitride membrane with refractive index $n = 2$ enhances linearly with the enhancement of corona charge, reaching above 24 V; When the refractive index n is 2.05 and 2.1, the surface electric tension of the silicon nitride membrane gradually enhances with the enhancement of the corona charge. When the corona charge reaches 2500 nC/cm² and 1000 nC/cm², the surface electric tension gradually reaches the limit value of 14 V and 1000 nC/cm², separately. About 7 V, when the refractive index n is 2.15 and 2.2, the surface electric tension of the silicon nitride

membrane reaches the limit electric tension when the corona charge is 500 nC/cm², and the surface electric tension does not change with the enhancement of the corona charge, and the two curves change. The trend is infinitely similar. For purpose of furthering touch bottom the impression of individual inactivation membranes on PID damping, a thermal oxidation furnace was used to feed 2000 sccm of oxygen at 950 °C, 990 °C, 1025 °C, and 1040 °C, and the process time was 50 minutes, and the refractive index $n = 1.416$ was stored, instances with SiO₂ membrane thickness of 19 nm, 37 nm, 45 nm, and 83 nm, separately. The batteries and small components are made by conventional science, and then PID test is carried out in the double 85 test box. The electrical capability parameters of the instances before and after PID testing are shown in tab. 3.

Table 3. Electrical capability parameter table of single-layer silicon oxide inactivation membrane before and after PID test

SiO ₂	PID	V _{oc} [V]	I _{sc} [A]	FF [%]	E _{ta} [%]	R _{sh} [Ω]	PID damping
19 nm	Before	0.61	8.44	67.47	14.28	12.7	7.35%
	After	0.60	7.92	67.88	13.23	12.2	
37 nm	Before	0.60	8.34	65.85	13.58	32.9	6.92%
	After	0.56	7.81	70.16	12.64	26.6	
45 nm	Before	0.59	7.73	66.16	12.31	43.8	5.76%
	After	0.58	7.37	66.35	11.60	44.2	
83 nm	Before	0.57	7.37	60.19	10.44	0.61	5.36%
	After	0.57	7.02	60.20	9.88	0.66	

From the data in tab. 3, it can be seen that after the same technical parameter's silicon wafers are stored with oxide membranes at individual temperatures to make cells, there are differences in cell conversion efficiency. The conversion efficiency decreased with the enhancement of the oxide membrane thickness. The higher the temperature, the greater the influence on the electrical capability, the open circuit electric tension, V_{oc} , and the short circuit current, I_{sc} . are gradually reduced. Due to the difference in the thickness of the silicon oxide membrane, the high temperature process leads to a large difference in the parallel resistance, R_{sh} , of the battery. After the PID test, the parallel resistance data first decreases slightly and then enhancements, which also shows that the leakage current gradually decreases with the enhancement of the oxide membrane thickness, so the PID decay is reduced.

Influence of double-layer silicon oxide/nitride inactivation membrane on PID damping

Aforementioned experiments have verified that the high refractive index silicon nitride membrane and the thick silicon oxide membrane have better inactivation effects, which can actually reduce the damping of PID. The investigation adopts the silicon oxide + silicon nitride double-layer membrane process to further touch bottom the influence of double-layer membrane on PID. Use a thermal oxidation furnace to deposit a silicon oxide membrane of about 10 nm, and then use a tubular PECVD to deposit a silicon nitride membrane, and deposit five communities of silicon oxide + silicon nitride with refractive indices of 2.00, 2.05, 2.10, 2.15, and 2.20, separately. For the sample, the amount membrane thickness was 85 nm. Then perform IV, EL, PID and other tests. The electrical capability parameters before and after the double-layer silicon oxide/silicon nitride PID were measured using an IV tester, as shown in tab. 4.

Table 4. Electrical capability parameter table of double-layer silicon oxide/silicon nitride inactivation membrane before and after PID

SiN _x /SiO ₂	PID	V_{oc} [V]	I_{sc} [A]	FF [%]	E_{ta} [%]	R_{sh} [Ω]	PID damping
2.00	Before	0.63	9.55	68.47	16.91	0.05	29.27%
	After	0.61	8.77	54.38	11.96	12.27	
2.05	Before	0.63	9.59	67.69	16.80	0.11	26.43%
	After	0.61	8.86	55.46	12.36	12.05	
2.10	Before	0.64	9.63	67.99	17.10	0.05	10.76%
	After	0.63	9.13	64.66	15.26	4.49	
2.15	Before	0.63	9.64	68.34	17.18	0.04	3.67%
	After	0.63	9.32	68.35	16.55	0.13	
2.20	Before	0.63	9.57	68.04	16.92	0.12	2.83%
	After	0.63	9.26	68.35	16.44	0.13	

It can be seen from tab. 4 that after the PID test of the five communities of instances, the open-circuit electric tension, V_{oc} , has almost no changes, the short-circuit current, I_{sc} , has decreased by 8.17%, 7.61%, 5.19%, 3.32%, and 3.24%, and the battery conversion efficiency has decreased by 29.27%, 26.43%, 10.76%, 3.67%, 2.83%, separately, all show a downward trend with the enhancement of the refractive index. Figure 5 compares the PID decay of the bilayer silicon oxide/silicon nitride membrane with that of the single layer silicon nitride membrane as a function of refractive index.

From fig. 5 that the PID damping trend of the double-layer membrane and the single-layer membrane is consistent. The PID damping decreases rapidly with the enhancement of the refractive index in the range of refractive index from 2.0 to 2.15. The damping is smaller. In

the range of refractive index 2.15 to 2.2, the PID damping curve tends to be stable, and the difference in power damping is small. It can be seen that the double-layer membrane has better anti-PID capability than the single-layer membrane. For purpose of touch bottom the data of the double 85 laboratorial box test PID, the PIDcon equipment was used to test the sample again. The relative changes in parallel resistance of instances of silicon oxide/silicon nitride membranes with individual refractive indices after PID testing are shown in fig. 6.

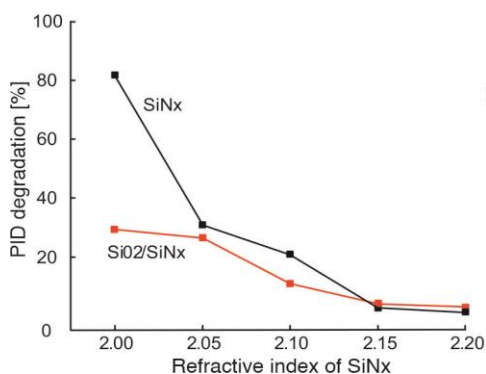


Figure 5. Variation of PID damping with refractive index for silicon nitride double-layer membrane and single-layer membrane

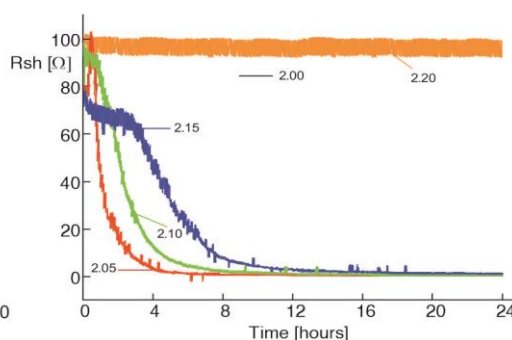


Figure 6. Relative change of parallel resistance of instances of silicon oxide/silicon nitride membranes with individual refractive indices after PID test

From fig. 6 that for instances with refractive indices of 2.05, 2.1, 2.15, and 2.20, under the conditions of a temperature of 85 °C and a reverse electric tension of 1500 V, the parallel resistance drops rapidly within 2 hours, and the curve of the sample with a refractive index of 2.0 tends to be stable. The curves of instances with refractive indices of 2.05, 2.1, and 2.15 tend to be stable after 4 hours, 8 hours, and 10 hours, separately, and the parallel resistance is basically close to zero. During the whole 24 hours test process of the refractive index 2.2 sample, there was little change at first, and the relative value of the parallel resistance was above 90. The power decay over time of instances of silicon oxide/silicon nitride membranes with individual refractive indices after PID testing is shown in fig. 7.

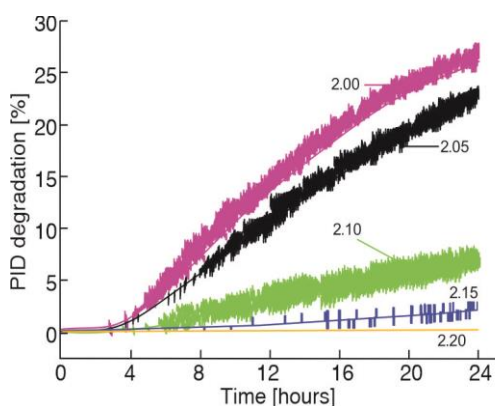


Figure 7. Variation of power with time after PID test of instances of silicon oxide/silicon nitride membranes with individual refractive indices

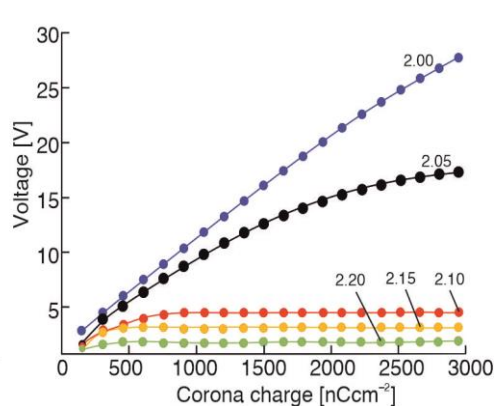


Figure 8. The VQ consequences of double-layer silicon oxide/silicon nitride membrane test

From fig. 7 that the power variation trend is consistent with the parallel resistance variation trend. For purpose of furthering touch bottom the reliability of the above proof consequences, the VQ tester from Semilab was used to test, and the VQ consequences of double-layer silicon oxide/silicon nitride were tested, as shown in fig. 8.

From fig. 8 that when the charging capacity is continuously enhanced from 0 to 3000 nC/cm², the surface electric tension of the bilayer membrane with refractive index $n = 2$ accelerates linearly with the advance of corona charge, and the limit electric tension reaches leave behind 30 V. When the refractive index n is 2.05, the surface electric tension of the double-layer membrane gradually enhancements with the enhancement of the corona charge. When the corona charge reaches 2500 nC/cm², the surface electric tension gradually reaches the limit value of 15 V. The refractive index n is 2.1, 2.15. At 2.2, the surface electric tension of the double-layer membrane reaches the limit electric tension when the corona charge is about 500 nC/cm². With the further enhancement of the corona charge, the surface electric tension does not change, and the curve trend is stable. When the surface electric tension reaches saturation, the forward charge that continues to be applied is extracted due to the leakage of the membrane itself, and does not contribute to the surface electric tension.

Conclusion

Based on the investigation on the PID capability damping of inactivation mediums for instance alumina/silicon nitride SiN for transparent silicon high-efficiency solar cells, it is found that the deposition approach of silicon oxide and silicon nitride inactivation membranes on the surface of transparent silicon cells directly affects the PID damping, and that the thermal oxide membrane is stronger than ozone. The oxide membrane at room temperature has high minority carrier lifetime and good anti-PID damping capability. Tubular PECVD has longer minority carrier lifetime and better anti-PID capability than plate PECVD stored silicon nitride inactivation membrane. When the thickness is constant, the single-layer silicon nitride membrane enhances with the refractive index and the anti-PID damping capability is gradually enhanced. When the refractive index is constant, when the thickness of the single-layer silicon oxide membrane enhancements from 19 nm to 83 nm, the anti-PID damping capability is gradually enhanced, and the single-layer silicon oxide membrane with the same thickness has better capability than the silicon nitride membrane. Anti-PID capability: As the refractive index of the double-layer silicon oxide/silicon nitride superimposed membrane enhancements, the anti-PID damping capability is gradually enhanced, and it has better anti-PID capability than single-layer silicon nitride. This may be because when the thickness of the inactivation membrane is thick or the density and refractive index are high. The leakage capability of the inactivation membrane is enhanced, but the charge accumulation ability on the battery surface is reduced. The surface electric tension is reduced, and the PID effect is weakened. Through investigation, many capabilities of solar cells can be improved, and further investigation can be carried out on more solar products in the future, and this kind of pure reproducible energy can be more fully applied to production and life.

Fundings

The research is supported by the National Key Research and Development Program of China (2022YFF0709501), National Natural Science Foundation of China (NSFC, Grant Nos. 12035020,52072399,62074165,12175305,62104253 and 12105357), Natural Science Foundation of Beijing Municipality (4192064,1212015).

Reference

- [1] Li, G., et al., Corrections to “Corrosion-Induced AC Impedance Elevation in Front Electrodes of Crystalline Silicon Photovoltaic Cells Within Field-Aged Photovoltaic Modules”, *IEEE Journal of Photovoltaics*, 9 (2019), 4, pp. 1154-1154
- [2] Yang, D., et al., Large Rea Luminescent Downshifting Layer Containing Eu³⁺ Complex for Crystalline Silicon Solar Cells, *Dalton Transactions*, 49 (2020), 15, pp. 4725-4731
- [3] Jonai, S., et al., Effect of Additives in Electrode Paste of P-Type Crystalline Si Solar Cells on Potential-Induced Degradation, *Solar Energy*, 188 (2019), Aug., pp. 1292-1297
- [4] Ahmad, A., et al., Photovoltaic Cell Defect Classification Using Convolutional Neural Network and Support Vector Machine, *IET Renewable Power Generation*, 14 (2020), 14, pp. 2693-2702
- [5] Niyaz, H. M., et al., Impact of Cracks on Crystalline Silicon Photovoltaic Modules Temperature Distribution, *Solar Energy*, 225 (2021), 11-12, pp. 148-161
- [6] Bouaichi, A., et al., Long-Term Experiment on P-Type Crystalline PV Module with Potential Induced Degradation: Impact on Power Performance and Evaluation of Recovery Mode, *Renewable Energy*, 183 (2022), C, pp. 472-479
- [7] Arfin, T., Arshiya Tarannum, K., Review on Detection of Phenol in Water, *Advanced Materials Letters*, 10 (2019), 11, pp. 753-785
- [8] Liang, S. X., et al., Study of the Remediation Effects of Passivation Materials on Pb-Contaminated Soil, *Open Chemistry*, 18 (2020), 1, pp. 911-917
- [9] Mishra, S., et al., Numerical Simulation of Potential Induced Degradation (PID) in Different Thin-Film Solar Cells Using SCAPS-1D, *Solar Energy*, 188 (2019), Aug., pp. 353-360
- [10] Kivik, P., et al., Measurement of Impedance of AGM Solar Battery for RAPS Applications, *ECS Transactions*, 105 (2021), 1, pp. 151-158
- [11] Shubhra, S., Singh, B., Three-Phase Grid-Interactive Solar PV-Battery Microgrid Control Based on Normalized Gradient Adaptive Regularization Factor Neural Filter, *IEEE Transactions on Industrial Informatics*, 16 (2020), 4, pp. 2301-2314
- [12] Salim, H. K., et al., Drivers, Barriers and Enablers to End-of-Life Management of Solar Photovoltaic and Battery Energy Storage Systems: A Systematic Literature Review, *Journal of Cleaner Production*, 211 (2019), Feb., pp. 537-554
- [13] Zare, F., et al., Applying Solar Energy in the Combination of Solar Dryer with Olive Harvesting Machine to Reduce Energy Losses, *Sustainability*, 14 (2022), 3, pp. 3751-3779
- [14] Cagle, A. E., et al., The Land Sparing, Water Surface Use Efficiency, and Water Surface Transformation of Floating Photovoltaic Solar Energy Installations, *Sustainability*, 12 (2020), 19, pp. 8154-8175
- [15] Noorollahi, Y., et al., A Spatial-Based Integration Model for Regional Scale Solar Energy Technical Potential, *Sustainability*, 12 (2020), 5, pp. 1890-1908
- [16] Singh, B., Knueven, B., Lagrangian Relaxation-Based Heuristics for a Chance-Constrained Optimization Model of a Hybrid Solar-Battery Storage System, *Journal of Global Optimization*, 80 (2021), 4, pp. 965-989
- [17] Chandran, V. P., et al., Multi-Objective Control and Operation of Grid Connected Small Hydro-SolarPV-Battery Energy Storage Based Distributed Generation, *IET Renewable Power Generation*, 14 (2020), 16, pp. 3259-3272
- [18] Sun, Z., et al., Performance-Enhancing Approaches for PEDOT: PSS-Si Hybrid Solar Cells, *Angewandte Chemie International Edition*, 60 (2021), 10, pp. 5036-5055
- [19] Ye, J., et al., Defect Passivation in Lead-Halide Perovskite Nanocrystals and Thin Films: Toward Efficient LEDs and Solar Cells, *Angewandte Chemie*, 133 (2021), 40, pp. 21804-21828
- [20] Li, Y., Wu, J., Optimum Integration of Solar Energy with Battery Energy Storage Systems, *IEEE Transactions on Engineering Management*, 69 (2020), 3, pp. 697-707